JMI Journal of Medical Imaging

RESEARCH PAPER

Data-driven abdominal phenotypes of type 2 diabetes in lean, overweight, and obese cohorts from computed tomography

Lucas W. Remedios,[a,*] Chloe Cho,[b] Trent M. Schwartz,[c] Dingjie Su,[a] Gaurav Rudravaram,[c] Chenyu Gao,[c] Aravind R. Krishnan,[c] Adam M. Saunders,[c] Michael E. Kim,[a] Shunxing Bao,[c] Alvin C. Powers,[d,e,f] Bennett A. Landman,[a,b,c] and John Virostko[g,h,i,j]

[a]Vanderbilt University, Department of Computer Science, Nashville, Tennessee, United States
[b]Vanderbilt University, Department of Biomedical Engineering, Nashville, Tennessee, United States
[c]Vanderbilt University, Department of Electrical and Computer Engineering, Nashville, Tennessee, United States
[d]Vanderbilt University Medical Center, Division of Diabetes, Endocrinology, and Metabolism, Department of Medicine, Nashville, Tennessee, United States
[e]Vanderbilt University, Department of Molecular Physiology and Biophysics, Nashville, Tennessee, United States
[f]VA Tennessee Valley Healthcare System, Nashville, Tennessee, United States
[g]University of Texas at Austin, Dell Medical School, Department of Diagnostic Medicine, Austin, Texas, United States
[h]University of Texas at Austin, Livestrong Cancer Institutes, Dell Medical School, Austin, Texas, United States
[i]University of Texas at Austin, Dell Medical School, Department of Oncology, Austin, Texas, United States
[j]University of Texas at Austin, Oden Institute for Computational Engineering and Sciences, Austin, Texas, United States

ABSTRACT. **Purpose:** Although elevated body mass index (BMI) is a well-known risk factor for type 2 diabetes, the disease's presence in some lean adults and absence in others with obesity suggests that more detailed measurements of body composition may uncover abdominal phenotypes of type 2 diabetes. With artificial intelligence (AI) and computed tomography (CT), we can now leverage robust image segmentation to extract detailed measurements of size, shape, and tissue composition from abdominal organs, abdominal muscle, and abdominal fat depots in 3D clinical imaging at scale. This creates an opportunity to empirically define body composition signatures linked to type 2 diabetes risk and protection using large-scale clinical data.

Approach: We studied imaging records of 1728 de-identified patients from Vanderbilt University Medical Center with BMI collected from the electronic health record. To uncover BMI-specific diabetic abdominal patterns from clinical CT, we applied our design four times: once on the full cohort ($n = 1728$) and once on lean ($n = 497$), overweight ($n = 611$), and obese ($n = 620$) subgroups separately. Briefly, our experimental design transforms abdominal scans into collections of explainable measurements, identifies which measurements most strongly predict type 2 diabetes and how they contribute to risk or protection, groups scans by shared model decision patterns, and links those decision patterns back to interpretable abdominal phenotypes in the original explainable measurement space of the abdomen using the following steps. (1) To capture abdominal composition: we represented each scan as a collection of 88 automatically extracted measurements of the size, shape, and fat content of abdominal structures using TotalSegmentator. (2) To learn key predictors: we trained a 10-fold cross-validated random forest classifier with SHapley Additive exPlanations (SHAP) analysis to rank features and estimate their risk-versus-protective effects for type 2 diabetes. (3) To validate

*Address all correspondence to Lucas W. Remedios, lucas.w.remedios@vanderbilt.edu

individual effects: for the 20 highest-ranked features, we ran univariate logistic regressions to quantify their independent associations with type 2 diabetes. (4) To identify decision-making patterns: we embedded the top-20 SHAP profiles with uniform manifold approximation and projection and applied silhouette-guided K-means to cluster the random forest's decision space. (5) To link decisions to abdominal phenotypes: we fit one-versus-rest classifiers on the original anatomical measurements from each decision cluster and applied a second SHAP analysis to explore whether the random forest's logic had identified abdominal phenotypes.

Results: Across the full, lean, overweight, and obese cohorts, the random forest classifier achieved a mean area under the receiver operating characteristic curve (AUC) of 0.72 to 0.74. SHAP highlighted shared type 2 diabetes signatures in each group—fatty skeletal muscle, older age, greater visceral and subcutaneous fat, and a smaller or fat-laden pancreas. Univariate logistic regression confirmed the direction of 14 to 18 of the top 20 predictors within each subgroup ($p < 0.05$). Clustering the model's decision space further revealed type 2 diabetes-enriched abdominal phenotypes within the lean, overweight, and obese subgroups.

Conclusions: We found similar abdominal signatures of type 2 diabetes across the separate lean, overweight, and obese groups, which suggests that the abdominal drivers of type 2 diabetes may be consistent across weight classes. Although our model had a modest AUC, the explainable components allowed for a clear interpretation of feature importance. In addition, in both lean and obese subgroups, the most important feature for identifying type 2 diabetes was fatty skeletal muscle.

© The Authors. Published by SPIE under a Creative Commons Attribution 4.0 International License. Distribution or reproduction of this work in whole or in part requires full attribution of the original publication, including its DOI. [DOI: 10.1117/1.JMI.12.6.064006]

Keywords: type 2 diabetes; phenotype; explainable artificial intelligence; abdomen; computed tomography; body composition; pattern discovery

Paper 25320GR received Aug. 14, 2025; revised Nov. 24, 2025; accepted Nov. 30, 2025; published Dec. 18, 2025.

1 Introduction

Type 2 diabetes is a chronic metabolic disease linked to alterations in body composition.[1–5] Although coarse measurements such as body mass index (BMI) and waist circumference are correlated with type 2 diabetes, the pattern of fat distribution is a stronger predictor of disease risk than overall adiposity.[6–8] Importantly, people with similar BMI can exhibit vastly different metabolic risk profiles. Some obese individuals remain type 2 diabetes-free (metabolically healthy obesity), whereas others with normal BMI develop type 2 diabetes.

In the type 2 diabetes population, changes have been noted across many anatomical structures. When compared to normal populations, there is evidence for higher body fat percent, more subcutaneous fat, more visceral fat, as well as less and fatty lean mass like skeletal muscle.[2,3,9–15] Although BMI defines obesity, closer examination has shown that in obese adults an increase in visceral fat is associated with type 2 diabetes.[13,16] In the abdominal organs, type 2 diabetes is associated with an increase in fat in the liver, pancreas, and kidneys, as well as a smaller pancreas.[13,17–26] Because low muscle mass is related to type 2 diabetes, it follows that resistance training has been shown to be associated with an improvement in blood sugar and insulin sensitivity.[27] However, there is some conflicting evidence from bioelectrical impedance analysis implying that lean mass is not protective of type 2 diabetes.[28,29]

Today, medical imaging and artificial intelligence (AI) make it possible to measure abdominal composition with unprecedented detail, scale, and interpretability.[30–34] These technologies pair well with ongoing research interest in large-scale examination of body composition and/or whole-body imaging.[35–39] Tools such as TotalSegmentator automatically segment over 100 anatomical structures in computed tomography (CT) or MRI scans, enabling large-scale extraction of organ volumes, fat distributions, and shape metrics without manual intervention.[40,41] When paired with explainable AI techniques such as SHapley Additive exPlanations (SHAP), predictive models built on these features can rank the importance of each anatomical measurement and quantify its directional influence on type 2 diabetes risk.[42] In this work, explainable AI refers to feature-attribution

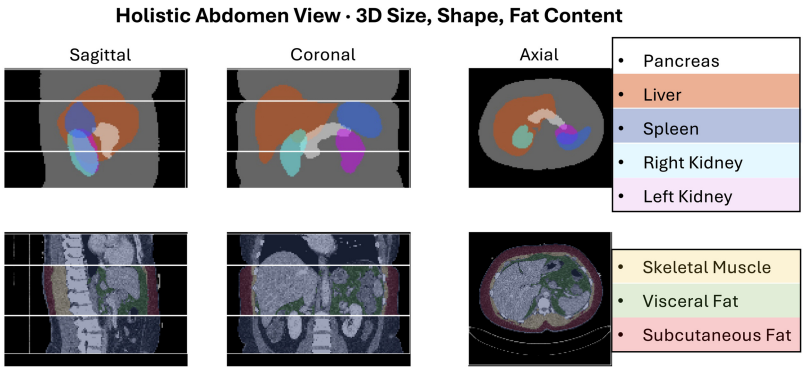


Fig. 1 AI-driven body composition analysis of large imaging datasets opens new avenues for data-driven discovery of abdominal phenotypes linked to metabolic risk, particularly by identifying which quantitative measurements, and which combinations of those measurements, most effectively distinguish individuals with type 2 diabetes from control patients. The anatomical labels shown reflect the maximum anatomical granularity provided by our selected segmentation model. Skeletal muscle and fat depots were cropped between the L2 and T10 vertebrae to enable consistent comparisons across diverse patients.

methods that clarify how individual input features contribute to a model's predictions, improving transparency for both clinicians and researchers. This explainability transforms AI from a black box into a tool for scientific discovery, both validating known relationships (e.g., high visceral fat increases risk) and revealing novel combinations that may not emerge from a purely hypothesis-driven analysis. In this context, data-driven modeling becomes a powerful means to help uncover new phenotypes and generate mechanistic validation of the literature.

Although considerable effort has been devoted to phenotyping specific organ systems and structures in type 2 diabetes, our work focuses on characterizing abdominal signatures of type 2 diabetes across separate lean, overweight, and obese groups. We use a holistic view of the abdomen to assess combinations of features to (1) rank feature importance for type 2 diabetes prediction, (2) discover multifeature signatures of type 2 diabetes, and (3) explore the model's decision-making landscape to investigate anatomical phenotypes (Fig. 1). Although our overall approach could extend to other modalities such as MRI, in this study, we focus on CT because attenuation values provide a convenient and widely used surrogate for tissue composition across organs, muscle, and fat depots.

2 Methods

We take heterogeneous clinical imaging data, represent each scan as a collection of abdominal measurements, and determine which patterns of features separate type 2 diabetes from control (Fig. 2). These images come from a diverse pool of clinical acquisitions, meaning that there is variability across protocols, image resolution, field of view, the use of contrast enhancement, and more. The computational system we have designed in this work connects validated tools into a pipeline for pattern discovery.

2.1 Data

Leveraging a culture of secondary data use,[43] we conducted a retrospective observational study on de-identified data from Vanderbilt University Medical Center under Institutional Review Board approval (IRB # 241494). After processing and quality assurance, detailed below, the dataset consisted of 1728 patients, aged 20 or older, each with a single clinically acquired CT scan of the abdomen.

Each of the 1728 scans successfully passed through the processing steps and quality assurance procedure detailed in the rest of this section. The medical images were converted from DICOM[44] to NiFTI[45] format using dcm2niix.[46] Scans were reoriented to standard orientation (LAS), manually inspected with AutoQA,[47] cropped between the L5 and T7 vertebrae (from TotalSegmentator vertebrae segmentation[40]), and resampled to 3 mm isotropic resolution to speed up downstream processing steps. We selected the target resolution of 3 mm as a middle ground because the resolution of the images ranged from 0.39 to 6 mm.

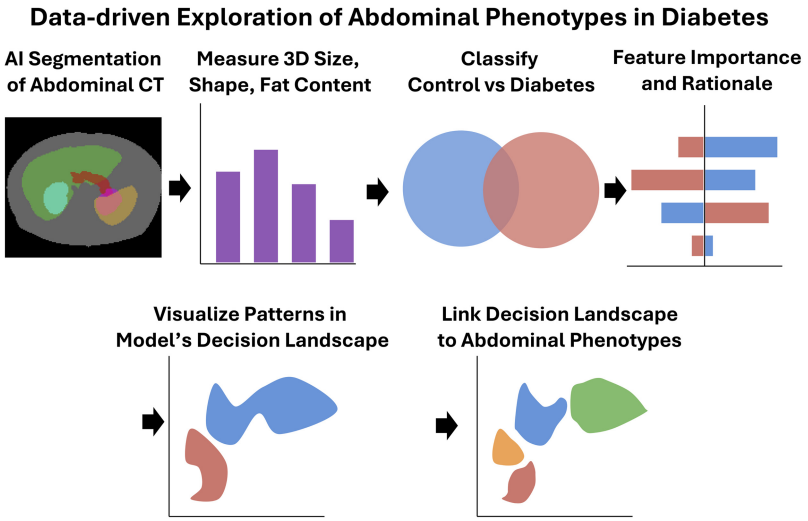


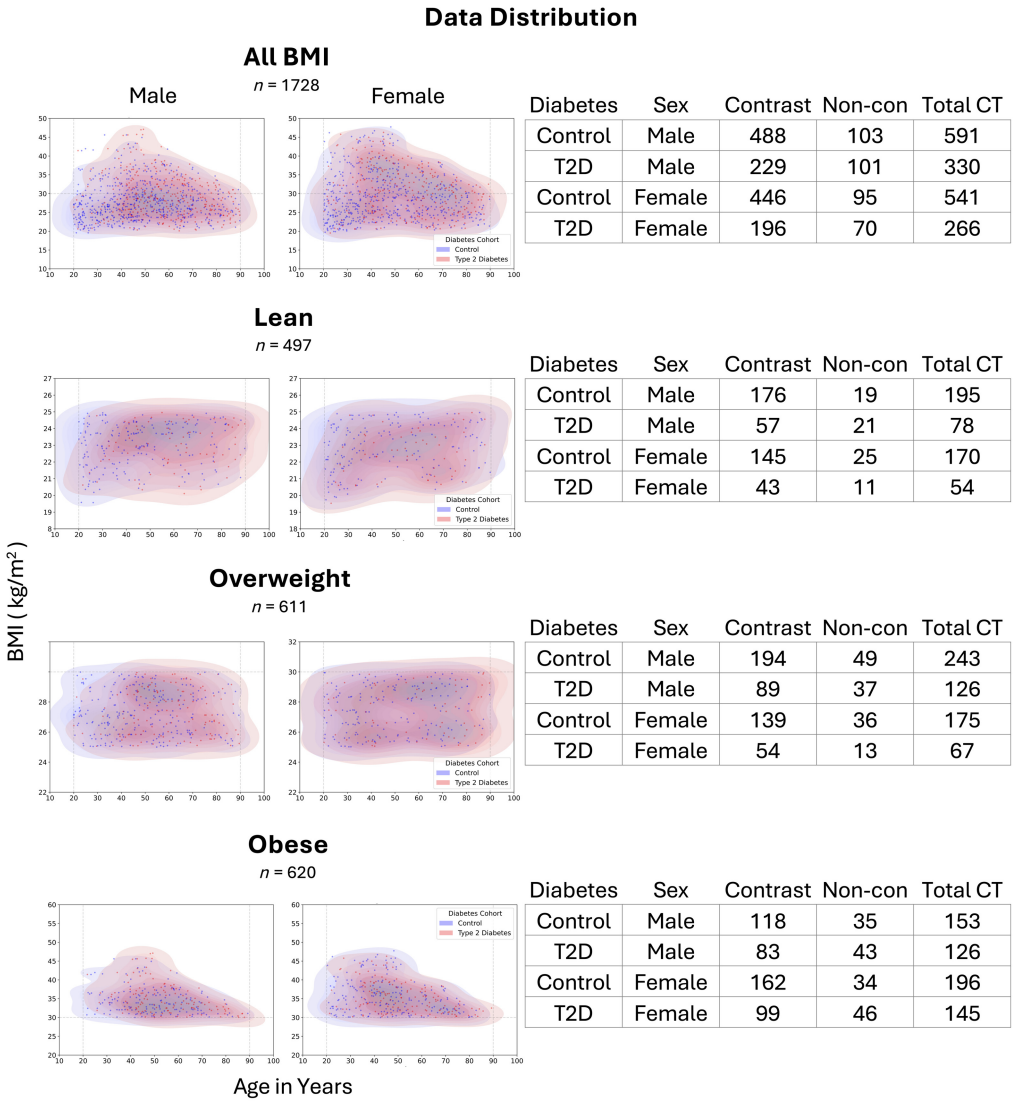
Fig. 2 Our approach for abdominal phenotyping leverages AI to represent the abdomen as a combination of 88 fully explainable 3D measurements, capturing the size, shape, and fat content of abdominal structures. We use predictive modeling with explainable AI techniques to characterize differences in the abdominal anatomy of individuals with type 2 diabetes. By mapping decisions from the predictive models back to anatomy, our pipeline functions both as a pattern-discovery engine, revealing emergent phenotypes, and a validation engine, highlighting where data-driven insights align with existing knowledge.

These preprocessed data were then fed to the CT model from TotalSegmentator[40] version 2.8 for automated segmentation of the pancreas, liver, spleen, right kidney, and left kidney. In addition, these data were segmented for visceral fat, subcutaneous fat, and skeletal muscle in an inferior-to-superior field of view between the middle of the L2 and T10 vertebrae. We created an explainable representation of the abdomen with 88 measurements by taking the eight segmentations, which delineate the abdominal structures in 3D, and extracting 11 size, shape, and CT Hounsfield unit density measurements: volume, surface area, surface-area-to-volume ratio, elongation, flatness, sphericity, major axis length, least axis length, minor axis length, maximum 3D diameter, and median intensity (median Hounsfield units on CT) with PyRadiomics[48] version 3.1. Median intensity of soft tissue on CT inversely correlates with fat content.[49] The scans in our dataset passed an extensive quality control pipeline, including the automatic exclusion of edge-touching segmentations (structures leaving the image field of view) and multi-island segmentations (more than one recognized object for structures that are one object), as well as several rounds of careful manual visual review of both images and segmentations to ensure high data quality and reliable measurements. Type 2 diabetes status was assigned from ICD/PhecodeX[50] records up to 1 year after imaging while excluding cases with cancer, pancreatic disease, sepsis, or trauma. CTs were automatically categorized as contrast-enhanced or noncontrast via TotalSegmentator's phase classifier and confirmed by visual inspection with the high-throughput AutoQA quality assurance tool.[47]

The patients studied in this work spanned ages 20 to 90 and were imaged for medical reasons rather than directly for body composition research. Due to the clinical setting, these images were not all acquired in a similar manner; however, through our preprocessing steps, we ensure the images capture the same 3D field of view covering the requisite anatomical region of the abdomen. These imaging data are a subset of the data used in a different study on the aging pancreas.[51] Supplemental details on the dataset can be found in the cited paper in Secs. 2.1–2.4[51] and include determination of binary label assignment for type 2 diabetes, inclusion criteria, and patient phenotypes. The metadata associated with these varied clinical images can tend to be sparse, so we do not include statistics about CT information, such as dose.

2.2 BMI-Based Subgrouping and Data Balancing

To investigate if abdominal patterns change in different BMI classes, we grouped our data into four cohorts: all BMI (all the data), lean (BMI < 25 kg/m^2), overweight (25 kg/m^2 $\leq$ BMI $<$



Diabetes	Sex	Contrast	Non-con	Total CT
Control	Male	488	103	591
T2D	Male	229	101	330
Control	Female	446	95	541
T2D	Female	196	70	266

Diabetes	Sex	Contrast	Non-con	Total CT
Control	Male	176	19	195
T2D	Male	57	21	78
Control	Female	145	25	170
T2D	Female	43	11	54

Diabetes	Sex	Contrast	Non-con	Total CT
Control	Male	194	49	243
T2D	Male	89	37	126
Control	Female	139	36	175
T2D	Female	54	13	67

Diabetes	Sex	Contrast	Non-con	Total CT
Control	Male	118	35	153
T2D	Male	83	43	126
Control	Female	162	34	196
T2D	Female	99	46	145

Fig. 3 Our balanced data support answering key scientific questions, such as (1) why some lean individuals develop type 2 diabetes and (2) why some obese individuals remain type 2 diabetes-free. We stratified a large dataset of patients with clinical CT of the abdomen into four groups: the full cohort (all BMI), lean (BMI < 25 kg/m^2), overweight (25 $kg/m^2 \leq$ BMI < 30 kg/m^2), and obese (BMI $\geq$ 30 kg/m^2). Within each subgroup, the BMI distributions over the age range were reasonably comparable between individuals with and without type 2 diabetes, visualized separately for males and females using both kernel density estimates and scatterplots. We included both non-contrast (noncon) and contrast (contrast-enhanced) CT to allow for a larger sample size from the varied clinical data. Contrast is relevant because it alters CT attenuation in abdominal structures, and many of our tissue-composition estimates (e.g., fat content) are derived from attenuation values within segmented structures.

30 kg/m^2), and obese (BMI $\geq$ 30 kg/m^2). These BMI groupings were selected following guidance from the World Health Organization. We present the data and demonstrate that the distributions were reasonably balanced across sex, BMI, and age (Fig. 3).

2.3 Assessing Separability, Feature Ranking, and Signatures of Type 2 Diabetes

To investigate the separability of control from type 2 diabetes based on our collection of abdominal measurements, we trained a random forest classifier under 10-fold cross-validation. We selected a random forest because it provides strongly interpretable feature attributions: tree-based models enable exact computation of SHAP values, whereas SHAP values for artificial neural

networks rely on approximate methods.[42,52] Our cross-validation data splits were stratified on the combination of type 2 diabetes label, sex, age in decades, and whether the CT had contrast. The inputs to the random forest were the 88 abdominal size, shape, and intensity features, along with confounders: sex, age, BMI, and CT contrast (contrast or noncontrast). The output of the model was an estimated probability of type 2 diabetes (0 mapped to control, 1 mapped to type 2 diabetes). The random forest used 300 estimators, a max depth of 10, and specified that a leaf node needed at least five examples. To address class imbalance on the type 2 diabetes label, we used balanced class weighting from scikit-learn's random forest class weight option during training.[53] Performance was measured via the area under the receiver operating characteristic curve (AUC), which was computed separately for each fold and averaged across folds. Each validation fold, where performance was measured, had ~10% of the total data.

To explain why the random forest made decisions, we used SHAP analysis. We concatenated the SHAP values across the 10 folds and then identified the top 20 most important features for the random forest to decide if our scans were from control or type 2 diabetes patients.

2.4 Independent Significance Testing of Model-Prioritized Features

To verify that the random forest's SHAP-ranked features were independently informative, we evaluated each of the top 20 measurements in a separate (univariate) logistic regression model while adjusting for key confounders—sex, age, BMI, and a binary CT-contrast indicator. These logistic regressions were fit on the entire dataset (no cross-validation) for each of the four cohorts separately. For every model, we calculated the odds ratio (OR), 95% confidence interval, and standard error. The p-values were corrected for multiple comparisons with the Benjamini–Hochberg false discovery rate (FDR) across the 20 tests in each BMI stratum, and features with adjusted $p < 0.05$ were deemed statistically significant after FDR correction. Finally, we compared the sign of each OR with the SHAP directionality to measure agreement between the multivariate random-forest findings and these confounder-controlled univariate analyses.

2.5 Measuring Emergent Phenotypes

To determine whether the random forest decision space contained distinct anatomical phenotypes, we first converted each scan's SHAP[42] profile (20 features) into a two-dimensional embedding with UMAP.[54,55] We then applied k-means[55,56] clustering to the UMAP coordinates, scanning $k = 2$ to 10 and automatically selecting the solution with the highest silhouette[56] score.

For every resulting cluster, we trained a one-versus-rest random forest classifier using the abdominal measurements and confounders (sex, age, BMI, and CT-contrast flag) to quantify how its anatomy differed from all other clusters. A second SHAP analysis on these models provided an interpretable signature of each cluster—i.e., the anatomical measurements that most strongly distinguished that decision group from the remainder of the cohort.

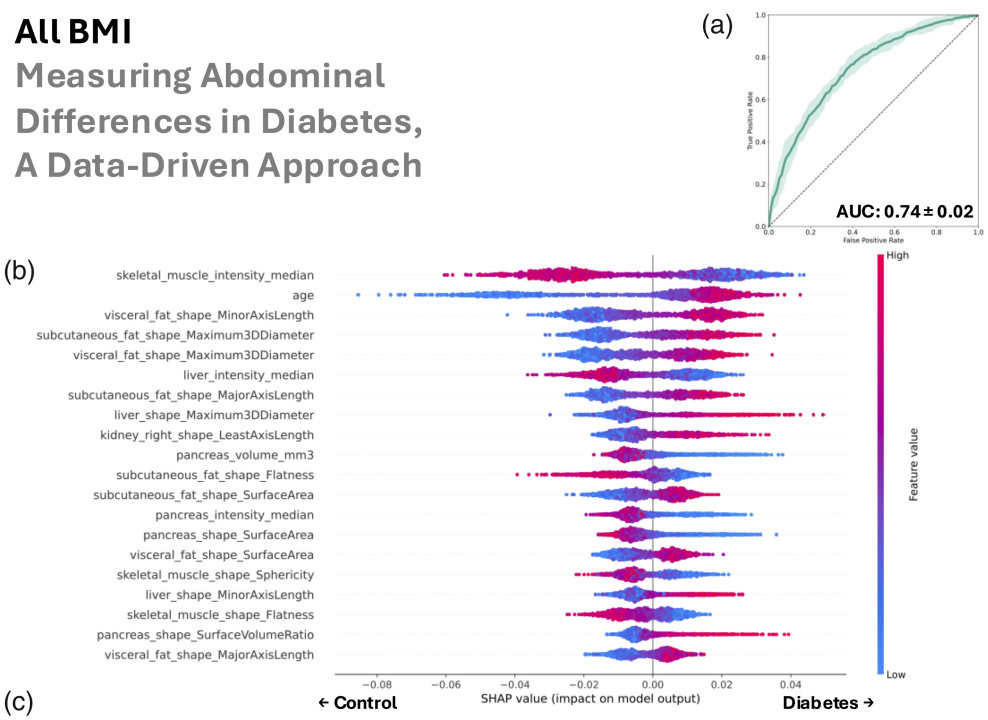
3 Results

3.1 Interpreting Model Decisions and Validating Feature Importance

In this section, we look sequentially at the four patient groupings (all BMI, lean, overweight, and obese) in Figs. 4–7.

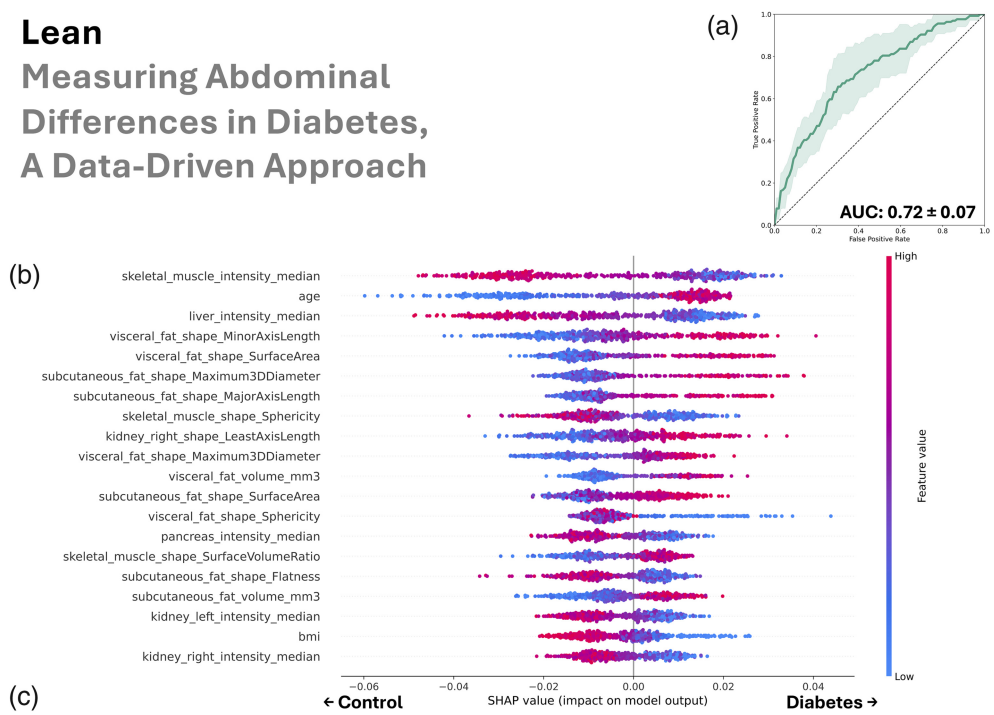
We used the AUC to assess our random forest's ability to distinguish type 2 diabetes from control patients via collections of their abdominal measurements. The mean AUCs ± standard deviation was 0.74 ± 0.02 for all BMI, 0.72 ± 0.07 for lean, 0.74 ± 0.04 for overweight, and 0.72 ± 0.06 for obese.

Our SHAP analysis of the random forest revealed both the ranking and directionality (risk versus protective) of the top 20 anatomical measurements used in model decisions. Shared patterns across BMI groups consistently associated with type 2 diabetes included fatty muscle (lower median HU intensity), older age, increased visceral and subcutaneous fat, and a smaller or fat-laden pancreas. A fatty and/or enlarged liver was informative for type 2 diabetes in all BMI, lean, and obese groups. Similarly, a smaller and/or fat-laden pancreas was important for predicting type 2 diabetes in those same groups. Right kidney enlargement contributed to classification toward type 2 diabetes in all BMI, lean, and overweight groups, whereas fatty kidneys (left and



Feature	OR	SE	95% CI	*p*-value	FDR-corrected p-value
skeletal_muscle_intensity_median	0.68	0.08	0.59 to 0.79	7.12E–07	1.42E–06 *
age	1.65	0.06	1.48 to 1.84	9.41E–20	1.88E–18 *
visceral_fat_shape_MinorAxisLength	1.69	0.07	1.46 to 1.96	1.30E–12	3.71E–12 *
subcutaneous_fat_shape_Maximum3DDiameter	1.84	0.08	1.58 to 2.16	1.99E–14	9.95E–14 *
visceral_fat_shape_Maximum3DDiameter	1.95	0.08	1.65 to 2.30	1.41E–15	9.43E–15 *
liver_intensity_median	0.69	0.08	0.59 to 0.81	5.58E–06	7.97E–06 *
subcutaneous_fat_shape_MajorAxisLength	1.86	0.08	1.58 to 2.18	4.05E–14	1.62E–13 *
liver_shape_Maximum3DDiameter	1.76	0.06	1.55 to 1.99	1.66E–18	1.66E–17 *
kidney_right_shape_LeastAxisLength	1.32	0.06	1.18 to 1.48	2.94E–06	4.86E–06 *
pancreas_volume_mm3	0.95	0.06	0.84 to 1.07	3.57E–01	3.57E–01
subcutaneous_fat_shape_Flatness	0.69	0.08	0.59 to 0.80	1.05E–06	1.91E–06 *
subcutaneous_fat_shape_SurfaceArea	1.65	0.08	0.40 to 1.94	2.19E–09	5.47E–09 *
pancreas_intensity_median	0.74	0.08	0.63 to 0.88	4.44E–04	5.22E–04 *
pancreas_shape_SurfaceArea	0.92	0.06	0.81 to 1.03	1.57E–01	1.65E–01
visceral_fat_shape_SurfaceArea	1.49	0.08	1.27 to 1.74	5.08E–07	1.13E–06 *
skeletal_muscle_shape_Sphericity	0.79	0.06	0.70 to 0.89	9.52E–05	1.27E–04 *
liver_shape_MinorAxisLength	1.53	0.06	1.36 to 1.73	9.16E–13	3.05E–12 *
skeletal_muscle_shape_Flatness	0.78	0.06	0.69 to 0.88	1.10E–04	1.37E–04 *
pancreas_shape_SurfaceVolumeRatio	1.17	0.06	1.04 to 1.31	8.17E–03	9.08E–03 *
visceral_fat_shape_MajorAxisLength	1.40	0.07	1.21 to 1.61	3.16E–06	4.86E–06 *

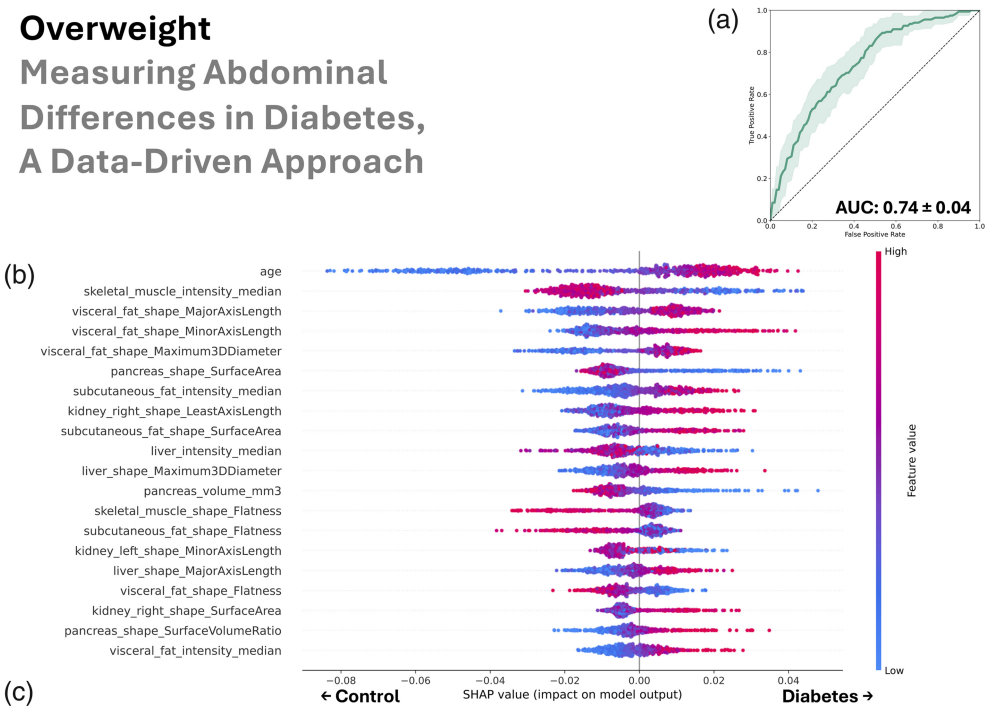
Fig. 4 Including all BMI groups, the data-driven abdominal phenotype of type 2 diabetes was characterized by reduced muscle density and sphericity, older age, greater visceral and subcutaneous fat, a fatty and enlarged liver, an enlarged right kidney, and a smaller fat-laden pancreas. (a) Random forest classifier distinguishes type 2 diabetes from controls (mean AUC 0.74). (b) SHAP ranking of the top 20 features shows the magnitude and direction of their risk or protective impact. (c) Univariate logistic regression confirms the same feature associations via odds ratios, with statistical significance denoted in green. We additionally color code blue for OR < 1 and red for OR > 1, which allows these features to be compared with the right half of the SHAP plot (b)—when an OR is blue, higher values of the feature are protective of type 2 diabetes, and when an OR is red, higher values are related with type 2 diabetes risk. In addition, in panel (c), SE denotes standard error, 95% CI denotes the 95% confidence interval, and FDR denotes false discovery rate.



(c)

Feature	OR	SE	95% CI	*p*-value	FDR-corrected p-value
skeletal_muscle_intensity_median	0.60	0.16	0.44 to 0.83	1.73E−03	3.14E−03 *
age	1.81	0.11	1.46 to 2.25	6.57E−08	1.31E−06 *
liver_intensity_median	0.45	0.18	0.31 to 0.64	9.84E−06	6.56E−05 *
visceral_fat_shape_MinorAxisLength	1.64	0.13	1.27 to 2.13	1.61E−04	4.03E−04 *
visceral_fat_shape_SurfaceArea	1.70	0.14	1.28 to 2.26	2.50E−04	5.55E−04 *
subcutaneous_fat_shape_Maximum3DDiameter	1.57	0.11	1.26 to 1.96	6.63E−05	1.95E−04 *
subcutaneous_fat_shape_MajorAxisLength	1.64	0.12	1.30 to 2.07	3.84E−05	1.53E−04 *
skeletal_muscle_shape_Sphericity	0.83	0.13	0.64 to 1.08	1.59E−01	1.76E−01
kidney_right_shape_LeastAxisLength	1.49	0.12	1.18 to 1.88	7.02E−04	1.40E−03 *
visceral_fat_shape_Maximum3DDiameter	1.91	0.15	1.43 to 2.57	1.62E−05	8.09E−05 *
visceral_fat_volume_mm3	1.48	0.13	1.14 to 1.92	3.36E−03	5.60E−03 *
subcutaneous_fat_shape_SurfaceArea	1.70	0.13	1.31 to 2.22	6.81E−05	1.95E−04 *
visceral_fat_shape_Sphericity	0.87	0.11	0.70 to 1.08	1.92E−01	2.03E−01
pancreas_intensity_median	0.66	0.17	0.47 to 0.91	1.23E−02	1.70E−02 *
skeletal_muscle_shape_SurfaceVolumeRatio	1.07	0.15	0.80 to 1.44	6.48E−01	6.48E−01
subcutaneous_fat_shape_Flatness	0.71	0.13	0.56 to 0.91	6.85E−03	1.05E−02 *
subcutaneous_fat_volume_mm3	1.85	0.13	1.42 to 2.41	5.13E−06	5.13E−05 *
kidney_left_intensity_median	0.65	0.17	0.46 to 0.91	1.28E−02	1.70E−02 *
bmi	0.79	0.11	0.63 to 0.97	2.84E−02	3.34E−02 *
kidney_right_intensity_median	0.69	0.17	0.50 to 0.96	2.66E−02	3.33E−02 *

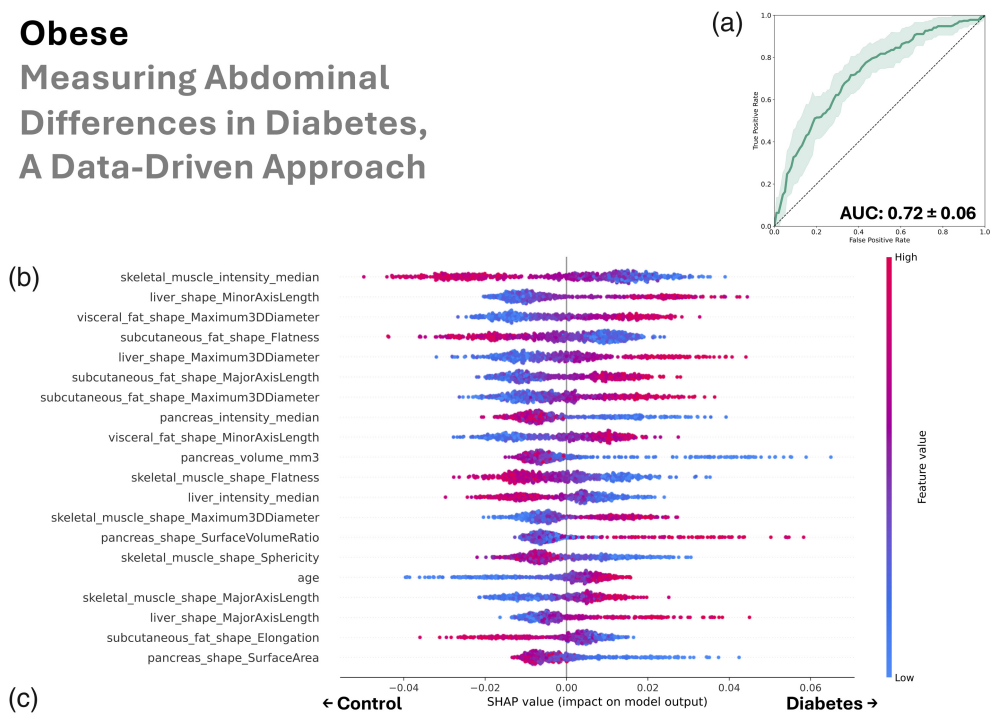
Fig. 5 In the lean group (BMI < 25 kg/m^2), the data-driven abdominal phenotype of type 2 diabetes was characterized by reduced muscle density and sphericity, older age, fatty liver, greater visceral and subcutaneous fat, enlarged right kidney, fat-laden pancreas, fatty left and right kidneys, and counterintuitively lower BMI. (a) Random forest classifier distinguishes type 2 diabetes from controls (mean AUC 0.72). (b) SHAP ranking of the top 20 features shows their risk or protective impact. (c) Univariate logistic regression confirms the same feature associations via odds ratios, with statistical significance denoted in green. We additionally color code blue for OR < 1 and red for OR > 1, which allows these features to be compared with the right half of the SHAP plot (b)—when an OR is blue, higher values of the feature are protective of type 2 diabetes, and when an OR is red, higher values are related with type 2 diabetes risk. In addition, in panel (c), SE denotes standard error, 95% CI denotes the 95% confidence interval, and FDR denotes false discovery rate.



(c)

Feature	OR	SE	95% CI	*p*-value	FDR-corrected *p*-value
age	1.73	0.09	1.44 to 2.08	5.73E−09	1.15E−07 *
skeletal_muscle_intensity_median	0.79	0.12	0.62 to 1.01	5.66E−02	7.35E−02
visceral_fat_shape_MajorAxisLength	1.32	0.11	1.07 to 1.64	1.07E−02	2.30E−02 *
visceral_fat_shape_MinorAxisLength	1.55	0.12	1.22 to 1.96	3.07E−04	1.53E−03 *
visceral_fat_shape_Maximum3DDiameter	1.51	0.12	1.19 to 1.92	7.19E−04	2.88E−03 *
pancreas_shape_SurfaceArea	0.78	0.10	0.64 to 0.95	1.48E−02	2.47E−02 *
subcutaneous_fat_intensity_median	1.35	0.09	0.13 to 1.63	1.23E−03	4.09E−03 *
kidney_right_shape_LeastAxisLength	1.31	0.10	1.08 to 1.60	6.94E−03	1.73E−02 *
subcutaneous_fat_shape_SurfaceArea	1.27	0.10	1.04 to 1.56	2.06E−02	3.17E−02 *
liver_intensity_median	0.83	0.13	0.64 to 1.06	1.36E−01	1.43E−01
liver_shape_Maximum3DDiameter	1.70	0.10	1.39 to 2.09	2.43E−07	2.43E−06 *
pancreas_volume_mm3	0.80	0.10	0.65 to 0.98	2.77E−02	3.95E−02 *
skeletal_muscle_shape_Flatness	0.85	0.10	0.69 to 1.04	1.12E−01	1.24E−01
subcutaneous_fat_shape_Flatness	0.83	0.10	0.67 to 1.01	6.89E−02	8.11E−02
kidney_left_shape_MinorAxisLength	1.02	0.10	0.84 to 1.24	8.48E−01	8.48E−01
liver_shape_MajorAxisLength	1.55	0.10	1.27 to 1.88	1.32E−05	8.79E−05 *
visceral_fat_shape_Flatness	0.83	0.10	0.69 to 1.01	5.88E−02	7.35E−02
kidney_right_shape_SurfaceArea	1.28	0.10	1.05 to 1.56	1.27E−02	2.30E−02 *
pancreas_shape_SurfaceVolumeRatio	1.28	0.10	1.06 to 1.56	1.25E−02	2.30E−02 *
visceral_fat_intensity_median	1.32	0.09	1.10 to 1.59	2.60E−03	7.42E−03 *

Fig. 6 In the overweight group (25 kg/m^2 ≤ BMI < 30 kg/m^2), the data-driven abdominal phenotype of type 2 diabetes was characterized by older age, reduced muscle density, greater and denser visceral and subcutaneous fat, reduced pancreas size, and enlarged right kidneys. (a) Random forest classifier distinguishes type 2 diabetes from controls (mean AUC 0.74). (b) SHAP ranking of the top 20 features shows their risk or protective impact. (c) Univariate logistic regression mostly agrees with the same feature associations via odds ratios, with statistical significance denoted in green. We additionally color code blue for OR < 1 and red for OR > 1, which allows these features to be compared with the right half of the SHAP plot (b)—when an OR is blue, higher values of the feature are protective of type 2 diabetes, and when an OR is red, higher values are related with type 2 diabetes risk. In addition, in panel (c), SE denotes standard error, 95% CI denotes the 95% confidence interval, and FDR denotes false discovery rate.



Feature	OR	SE	95% CI	p-value	FDR-corrected p-value
skeletal_muscle_intensity_median	0.68	0.11	0.55 to 0.85	6.70E−04	9.58E−04 *
liver_shape_MinorAxisLength	1.67	0.10	1.38 to 2.02	9.86E−08	2.82E−07 *
visceral_fat_shape_Maximum3DDiameter	2.30	0.13	1.77 to 2.97	3.23E−10	2.81E−09 *
subcutaneous_fat_shape_Flatness	0.68	0.10	0.56 to 0.83	1.14E−04	2.07E−04 *
liver_shape_Maximum3DDiameter	1.94	0.10	1.58 to 2.38	3.15E−10	2.81E−09 *
subcutaneous_fat_shape_MajorAxisLength	2.11	0.12	1.66 to 2.67	6.48E−10	3.24E−09 *
subcutaneous_fat_shape_Maximum3DDiameter	2.15	0.12	1.69 to 2.73	4.21E−10	2.81E−09 *
pancreas_intensity_median	0.69	0.13	0.54 to 0.89	4.33E−03	5.41E−03 *
visceral_fat_shape_MinorAxisLength	1.87	0.12	1.47 to 2.38	3.13E−07	7.50E−07 *
pancreas_volume_mm3	1.02	0.10	0.84 to 1.23	8.57E−01	8.57E−01
skeletal_muscle_shape_Flatness	0.70	0.10	0.58 to 0.85	2.64E−04	4.40E−04 *
liver_intensity_median	0.78	0.12	0.62 to 0.97	2.91E−02	3.43E−02 *
skeletal_muscle_shape_Maximum3DDiameter	1.97	0.13	1.54 to 2.53	9.88E−08	2.82E−07 *
pancreas_shape_SurfaceVolumeRatio	1.14	0.09	0.95 to 1.37	1.61E−01	1.78E−01
skeletal_muscle_shape_Sphericity	0.74	0.09	0.62 to 0.88	8.75E−04	1.17E−03 *
age	1.53	0.09	1.28 to 1.83	3.03E−06	6.07E−06 *
skeletal_muscle_shape_MajorAxisLength	2.12	0.14	1.62 to 2.78	3.74E−08	1.50E−07 *
liver_shape_MajorAxisLength	1.67	0.10	1.37 to 2.04	3.38E−07	7.50E−07 *
subcutaneous_fat_shape_Elongation	0.73	0.09	0.61 to 0.87	3.47E−04	5.34E−04 *
pancreas_shape_SurfaceArea	0.96	0.10	0.79 to 1.16	6.47E−01	6.81E−01

Fig. 7 In the obese group (BMI $\geq$ 30 kg/m^2), the data-driven abdominal phenotype of type 2 diabetes was characterized by reduced muscle density and sphericity, enlarged and fatty liver, increased visceral and subcutaneous fat, sometimes a smaller and fat-laden pancreas, and older age. (a) Random forest classifier distinguishes type 2 diabetes from controls (mean AUC 0.72). (b) SHAP ranking of the top 20 features shows their risk or protective impact. (c) Univariate logistic regression mostly agrees on the same feature associations via odds ratios, with statistical significance denoted in green. We additionally color code blue for OR < 1 and red for OR > 1, which allows these features to be compared with the right half of the SHAP plot (b)—when an OR is blue, higher values of the feature are protective of type 2 diabetes, and when an OR is red, higher values are related with type 2 diabetes risk. In addition, in panel (c), SE denotes standard error, 95% CI denotes the 95% confidence interval, and FDR denotes false discovery rate.

right) were relevant for type 2 diabetes prediction in the lean group. In the overweight group, the model predicted type 2 diabetes where there was a higher density in both visceral and subcutaneous fat. In the lean group, lower BMI was paradoxically used by the model to predict type 2 diabetes, suggesting that lean individuals with type 2 diabetes may have reduced muscle mass rather than fat.

Although our cross-validated random forest leveraged combinations of features to rank their importance and assign risk-versus-protective directionality, we independently validated each top feature with univariate logistic regression performed on the full dataset for every BMI subgroup (no cross-validation). The logistic regression odds-ratio direction (type 2 diabetes risk if > 1, protective if < 1) showed near-perfect concordance with the random forest SHAP findings. Moreover, after multiple comparisons correction, 18 of 20 features were significant in the all BMI group, 17 in the lean group, 14 in the overweight group, and 17 in the obese group. Because these univariate tests examined features in isolation, their general agreement with the multivariate random-forest results implies that the directionality of feature relationships with type 2 diabetes was robust across both univariate and multivariate models. In addition, we note that the

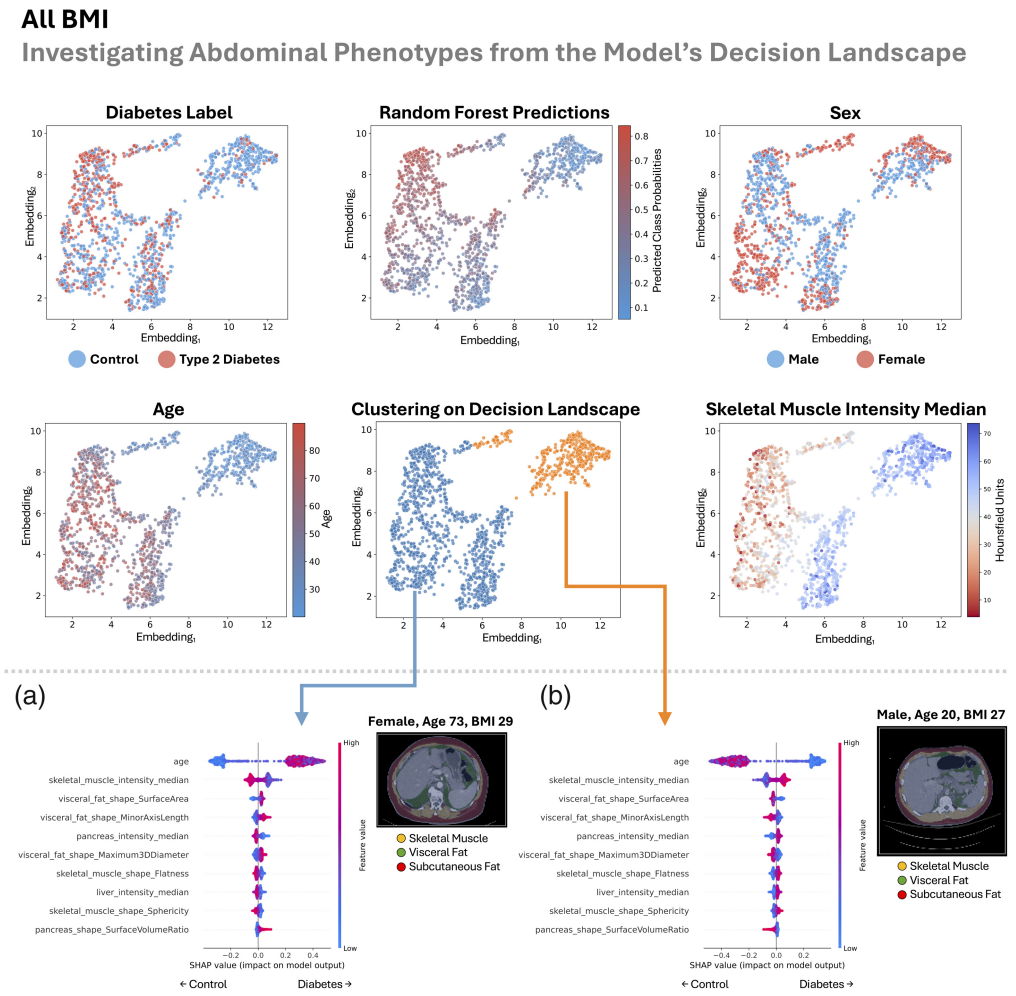


Fig. 8 Across all BMI groups, we inspect the landscape of the random forest's decision-making approach (upper half). There is reasonable agreement between the gradient of type 2 diabetes labels and our model's predictions. The decision space is strongly informed by age and muscle density but is not driven by sex differences. Mapping decision clusters back to anatomical space, we identify a type 2 diabetes-enriched signature (a) that is characterized by older age, worsened muscle density and shape, increased visceral fat, and a fatty pancreas with a high surface-area-to-volume ratio. We see the inverse phenotype in the control patient-enriched cluster (b). We additionally visualize the abdomen from the center scan in each cluster (minimum Euclidean distance to cluster centroid).

p-values from the univariate logistic regressions for the all BMI group (Fig. 4) were substantially smaller than for the subgroups: lean, overweight, and obese (Figs. 5–7). These very small p-values imply that the associations are unlikely to have occurred by chance. Their magnitudes align with the trends from the SHAP analysis on the random forests and are likely due to the much larger sample size in the all BMI group.

3.2 Linking Model Decisions to Abdominal Phenotypes

In this section, we look sequentially at the four patient groupings (all BMI, lean, overweight, and obese) in Figs. 8–11. Previously, we looked at overall patterns that explained how our random forest decided if a patient had type 2 diabetes based on explainable measurements of their abdomen. Here, we look for abdominal phenotypes or anatomical signatures in the random forest's decision space that cued the model to predict control or type 2 diabetes. We do this by looking at the top 20 abdominal measurements identified from the SHAP analysis as described in Sec. 2.5. This enables the opportunity to discover different abdominal patterns that lead to the same model decision, which could validate or potentially uncover different mechanisms of type 2 diabetes.

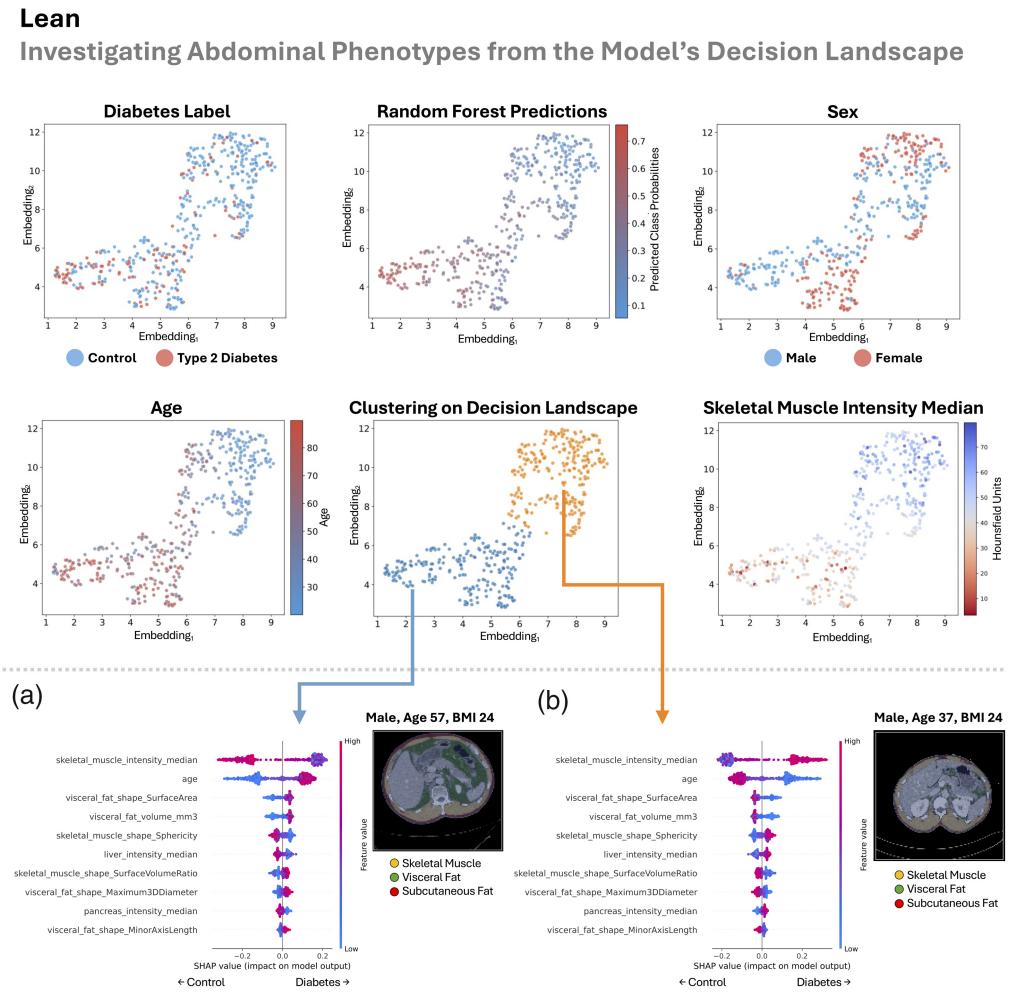


Fig. 9 In the lean group (BMI < 25 kg/m^2), we inspect the landscape of the random forest's decision-making approach (upper half). There is reasonable agreement between the gradient of type 2 diabetes labels and our model's predictions. The decision space is strongly informed by age and muscle density but is not driven by sex differences. Mapping decision clusters back to anatomical space, we identify a type 2 diabetes-enriched signature (a) that is characterized by worsened muscle density and shape, older age, increased visceral fat, fatty liver, and a fatty pancreas. We see the inverse phenotype in the control patient-enriched cluster (b). We additionally visualize the abdomen from the center scan in each cluster (minimum Euclidean distance to cluster centroid).

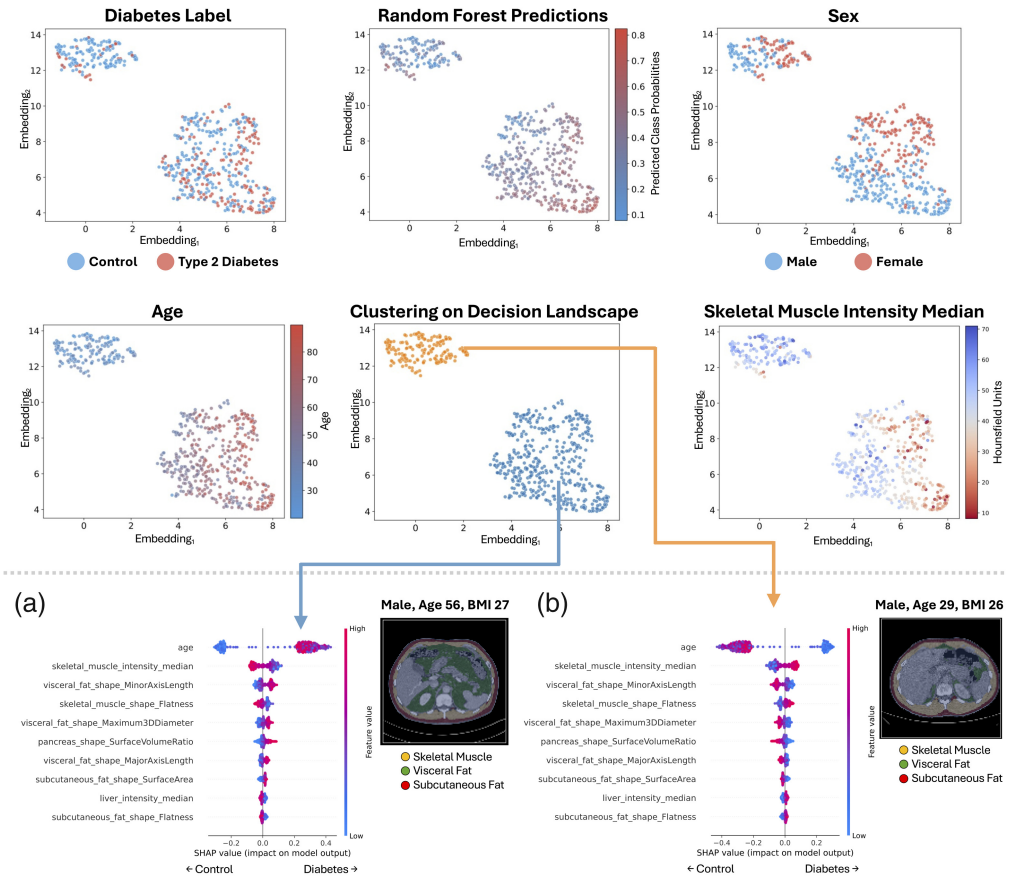


Fig. 10 In the overweight group (25 kg/m^2 ≤ BMI < 30 kg/m^2), we inspect the landscape of the random forest's decision-making approach (upper half). There is reasonable agreement between the gradient of type 2 diabetes labels and our model's predictions. The decision space is strongly informed by age and muscle density but is not driven by sex differences. Mapping decision clusters back to anatomical space, we identify a type 2 diabetes-enriched signature (a) that is characterized by older age, worsened muscle density and shape, increased visceral fat, increased subcutaneous fat, increased pancreas surface-area-to-volume ratio, and a fatty liver. We see the inverse phenotype in the control patient-enriched cluster (b). We additionally visualize the abdomen from the center scan in each cluster (minimum Euclidean distance to cluster centroid).

In all the groups, as we look across the decision landscape, there is reasonable agreement between the gradient of type 2 diabetes labels and our model's predictions (Figs. 8–11). Across groups, the decision space is strongly informed by age and muscle density (lower median HU) but is not driven by sex differences (all BMI, lean, and overweight) or partially driven by sex differences (obese).

Separately in each of the BMI, lean, and overweight cohorts, our method split patients into two decision clusters—one enriched for type 2 diabetes and the other for controls—with opposing anatomical signatures. In the type 2 diabetes-enriched clusters, we consistently observed poorer muscle density (lower median HU) and shape, older age, and greater visceral fat. In addition, type 2 diabetes-associated traits included a fatty pancreas in all BMI and lean groups, a fatty liver in lean and overweight groups, an elevated pancreas surface-area-to-volume ratio in all BMI and overweight groups, and increased subcutaneous fat in the overweight group.

The obese group was automatically divided into four distinct clusters, some of which reflected sex-based anatomical patterns. One cluster was enriched for type 2 diabetes and predominantly female, characterized by a smaller, fatty pancreas, older age, reduced muscle density and mass, and a smaller liver. Another type 2 diabetes- and male-enriched cluster, with an

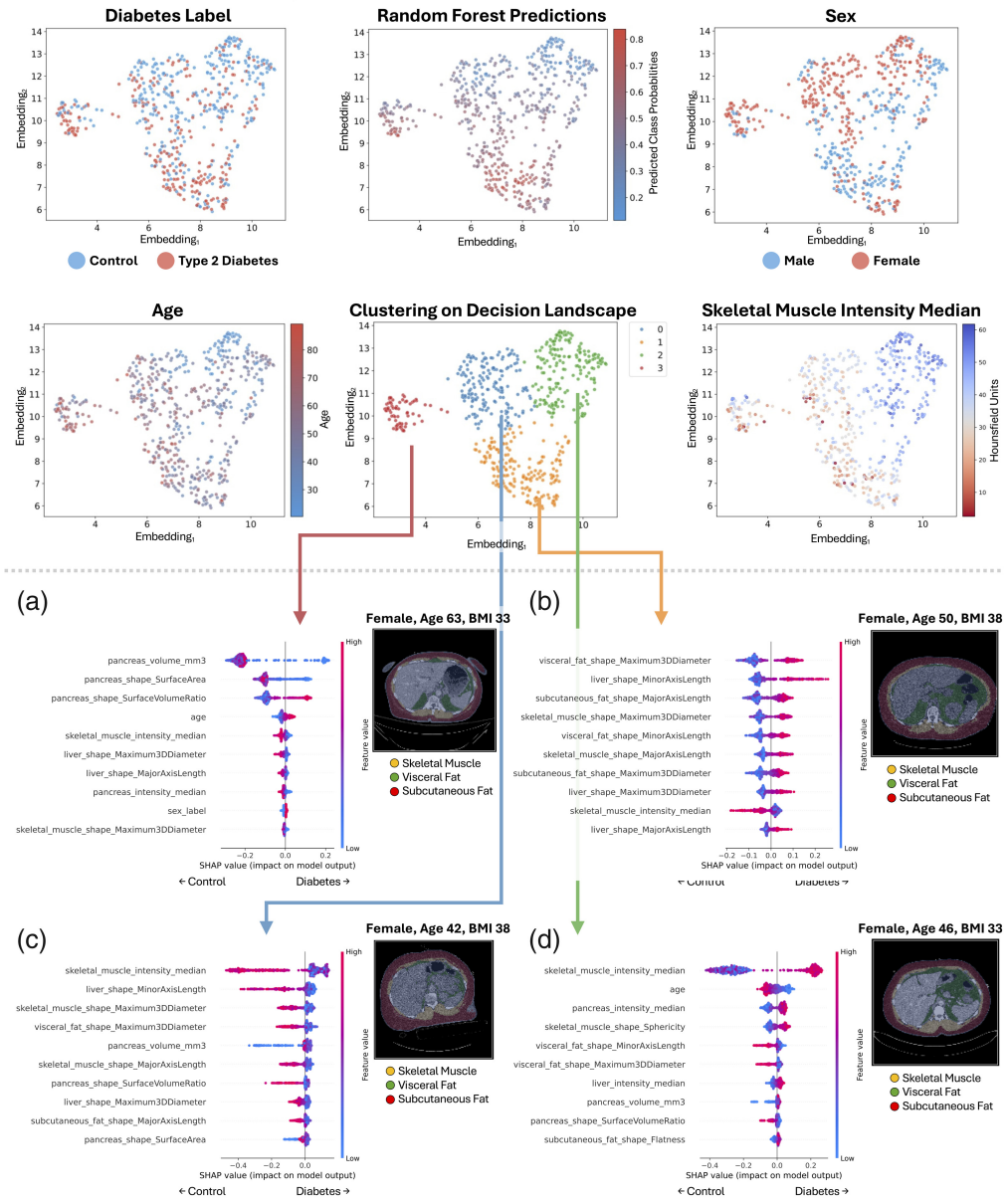


Fig. 11 In the obese group (BMI > 30 kg/m^2), we inspect the landscape of the random forest's decision-making approach (upper half). There is reasonable agreement between the gradient of type 2 diabetes labels and our model's predictions. The decision space is strongly informed by age and muscle density and partially driven by sex differences. Mapping decision clusters back to anatomical space, we identify a type 2 diabetes- and female-enriched signature (a) that is characterized by a smaller fatty pancreas, older age, reduced muscle density and mass, and a smaller liver. In panel (b), we identify a type 2 diabetes- and male/large-body-enriched signature that is characterized by increased visceral fat, increased liver size, increased subcutaneous fat, increased skeletal muscle, and reduced muscle density. In panel (c), we identify a control- and female-enriched signature that is characterized by worsened muscle density and size, smaller liver, reduced visceral and subcutaneous fat, and a sometimes smaller pancreas with a low surface-area-to-volume ratio. In panel (d), we identify a control-enriched cluster that is characterized by better muscle density and shape, lower age, a larger nonfatty pancreas, reduced visceral fat and flatter subcutaneous fat, and a nonfatty liver.

implied larger body size, showed increased visceral fat, larger liver, greater subcutaneous fat, increased skeletal muscle, and reduced muscle density. Among the control-enriched clusters, one was predominantly female and marked by reduced muscle density and size, a smaller liver, lower visceral and subcutaneous fat, and a sometimes smaller pancreas with a low surface-area-to-volume ratio. The other control-enriched cluster featured better muscle density and shape, younger age, a larger nonfatty pancreas, reduced visceral fat, flatter subcutaneous fat, and a nonfatty liver.

4 Discussion

By leveraging explainable machine learning, we uncovered multifeature anatomical profiles associated with type 2 diabetes and demonstrated that exploring the model's decision space enables automatic identification of clinically meaningful phenotypes directly within the anatomical measurement space. These findings support a shift toward comprehensive, data-driven characterization of type 2 diabetes risk and phenotype signatures.

The type 2 diabetes classification random forests were not exceptional diagnostic models (mean AUCs 0.72 to 0.74); an AUC of 0.5 is akin to random chance, and an AUC of 1.0 is a perfect classifier. However, these random forests had reasonable AUCs for biological pattern discovery. In the literature, AUCs near 0.7 are acceptable in the context of image-based models of metabolic disease.[6,57] Our AUC range was not surprising because we were classifying patients based only on measurements of their abdomen, sex, age, BMI, and contrast flag, but not including more powerful clinical measurements of blood glucose or medications.

Our data-driven signature of type 2 diabetes agreed with findings in the literature specifying that, when compared with normal, there is more subcutaneous fat, more visceral fat, and more fatty lean mass.[2,3,9–15] In addition, our type 2 diabetes signature shows concordance with the field on fatty liver, fatty pancreas, smaller pancreas, and sometimes fatty kidneys.[13,17–26] Our signature highlights the importance of fatty skeletal muscle in predicting type 2 diabetes across the board, which directly contrasts some of the bioelectrical impedance analysis literature that states lean mass is not protective of type 2 diabetes.[28,29] A limitation of our data-driven interpretation is that descriptors such as "larger," "smaller," or "fattier" reflect relative associations identified by the SHAP analysis within our cohort, rather than absolute clinical thresholds.

Our findings suggest that image-based phenotyping may support type 2 diabetes risk profiling from secondary use of CT scans acquired for other clinical purposes. Our study focused on data from one site. Future work should explore the generalizability of such type 2 diabetes risk profiling approaches across imaging sites, ultimately evaluating their potential for broader clinical utility. In addition, ratios of abdominal measurements from structures such as visceral fat and subcutaneous fat may offer complementary insights and represent an interesting direction for future work.

5 Conclusion

Our study identified type 2 diabetes patterns in the abdomen that were largely consistent with the literature. Separately for lean, overweight, and obese groups, fatty skeletal muscle emerged as either the most or second most important predictor, underscoring its central role in type 2 diabetes. Moreover, we found that the abdominal patterns of type 2 diabetes were largely the same across the separate lean, overweight, and obese groups, suggesting shared anatomical signatures of type 2 diabetes despite BMI class. Although we focused on type 2 diabetes in this work, our phenotyping methodology could be applied for pattern discovery in other disease domains.

Disclosures

The authors declare that there are no financial interests, commercial affiliations, or other potential conflicts of interest that could have influenced the objectivity of this research or the writing of this paper.

Code and Data Availability

The data that support the findings of this article are not publicly available.

Acknowledgments

This work was supported by Integrated Training in Engineering and Diabetes (Grant Nos. T32 DK101003 and MSTP T32) and the NIH NIGMS (Grant No. T32GM007347). This work used REDCap and VCTRS resources, which are supported by the National Center for Advancing Translational Sciences, National Institutes of Health (NIH) (Grant No. UL1 TR000445). These studies benefited from the infrastructure of the Vanderbilt Diabetes Research and Training Center (Grant No. DK 020593), Division of Diabetes, Endocrinology, and Metabolic Diseases, and the Vanderbilt University Institute of Imaging Science Center for Human Imaging (Grant No. 1 S10OD021771 01). This work was supported by NSF career (Grant Nos. 1452485 and 2040462). This work was supported by the Alzheimer's Disease Sequencing Project Phenotype Harmonization Consortium (ADSP-PHC), which is funded by NIA (Grant Nos. U24 AG074855, U01 AG068057, and R01 AG059716). This work was conducted in part using the resources of the Advanced Computing Center for Research and Education at Vanderbilt University, Nashville, TN. The Vanderbilt Institute for Clinical and Translational Research (VICTR) is funded by the National Center for Advancing Translational Sciences (NCATS) Clinical Translational Science Award (CTSA) Program (Award No. 5UL1TR002243-03). The content is solely the responsibility of the authors and does not necessarily represent the official views of the NIH. This work was supported by DoD (Grant No. HT94252410563). We extend gratitude to NVIDIA for their support by means of the NVIDIA hardware grant. This research was funded by the National Cancer Institute (NCI) (Grant Nos. R01 CA253923-04 and R01 CA 253923-04S1). Financial support was graciously provided by the National Institutes of Health (Grant Nos. DK129979 and HD115565) and Breakthrough T1D (formerly JDRF) (Grant No. 1-INO-2023-1340-A-N). We gratefully acknowledge philanthropic support from Thomas J. and Karen K. Gentry. The study sponsors were not involved in the design of the study and did not impose any restrictions regarding the publication of the report. We have used AI as a tool in the creation of this content; however, the foundational ideas, underlying concepts, and original gist stem directly from the personal insights, creativity, and intellectual effort of the authors. The use of generative AI serves to enhance and support the author's original contributions by assisting in the ideation, drafting, and refinement processes. All AI-assisted content has been carefully reviewed, edited, and approved by the authors to ensure it aligns with the intended message, values, and creativity of the work.

References

1. S. Sbrignadello, C. Göbl, and A. Tura, "Bioelectrical impedance analysis for the assessment of body composition in sarcopenia and type 2 diabetes," *Nutrients* **14**(9), 1864 (2022).
2. J. Gómez-Ambrosi et al., "Body adiposity and type 2 diabetes: increased risk with a high body fat percentage even having a normal BMI," *Obesity* **19**(7), 1439–1444 (2011).
3. J. Solanki et al., "Body composition in type 2 diabetes: change in quality and not just quantity that matters," *Int. J. Prev. Med.* **6**(1), 122 (2015).
4. S. Heshka et al., "Altered body composition in type 2 diabetes mellitus," *Int. J. Obes.* **32**(5), 780–787 (2008).
5. L. Müller, "AI-based body composition measures in abdominal CT scans: prime time for clinical implementation?," *Eur. Radiol.* **35**(1), 517–519 (2024).
6. Y. Chang et al., "Automated comprehensive CT assessment of the risk of diabetes and associated cardiometabolic conditions," *Radiology* **312**(2), e233410 (2024).
7. C. Li et al., "Evaluation for performance of body composition index based on quantitative computed tomography in the prediction of metabolic syndrome," *Metab. Syndr. Relat. Disord.* **22**(4), 287–294 (2024).
8. A. Marcadenti et al., "Adiposity phenotypes are associated with type-2 diabetes: LAP index, body adiposity index, and neck circumference," *Atherosclerosis* **266**, 145–150 (2017).
9. M. E. Al-Sofiani, S. S. Ganji, and R. R. Kalyani, "Body composition changes in diabetes and aging," *J. Diabetes Complications* **33**(6), 451–459 (2019).
10. M. C. Carr and J. D. Brunzell, "Abdominal obesity and dyslipidemia in the metabolic syndrome: importance of type 2 diabetes and familial combined hyperlipidemia in coronary artery disease risk," *J. Clin. Endocrinol. Metab.* **89**(6), 2601–2607 (2004).
11. O. Juntila et al., "Analytic morphomics describes body composition associated with diabetes," *Michigan J. Med.* **2**(1), 51–59 (2017).
12. Y. H. Kim et al., "Artificial intelligence-based body composition analysis using computed tomography images predicts both prevalence and incidence of diabetes mellitus," *J. Diabetes Investig.* **16**(2), 272–284 (2025).

13. T. Tirkes et al., "Association of pancreatic steatosis with chronic pancreatitis, obesity, and type 2 diabetes mellitus," *Pancreas* **48**(3), 420–426 (2019).
14. K. E. Bell et al., "Altered features of body composition in older adults with type 2 diabetes and prediabetes compared with matched controls," *J. Cachexia Sarcopenia Muscle* **13**(2), 1087–1099 (2022).
15. T. S. Han et al., "Associations of BMI, waist circumference, body fat, and skeletal muscle with type 2 diabetes in adults," *Acta Diabetol.* **56**(8), 947–954 (2019).
16. I. J. Neeland et al., "Dysfunctional adiposity and the risk of prediabetes and type 2 diabetes in obese adults," *JAMA* **308**(11), 1150 (2012).
17. D. H. Lee et al., "Comparison of the association of predicted fat mass, body mass index, and other obesity indicators with type 2 diabetes risk: two large prospective studies in US men and women," *Eur. J. Epidemiol.* **33**(11), 1113–1123 (2018).
18. C. Diamond et al., "Quantitative imaging reveals steatosis and fibroinflammation in multiple organs in people with type 2 diabetes: a real-world study," *Diabetes* **73**(8), 1285–1299 (2024).
19. H. Tallam et al., "Fully automated abdominal CT biomarkers for type 2 diabetes using deep learning," *Radiology* **304**(1), 85–95 (2022).
20. Q. An et al., "Association between type 2 diabetes mellitus and body composition based on MRI fat fraction mapping," *Front. Public Health* **12**, 1332346 (2024).
21. M. Macauley et al., "Altered volume, morphology and composition of the pancreas in type 2 diabetes," *PLoS One* **10**(5), e0126825 (2015).
22. Y. Saisho et al., "Pancreas volumes in humans from birth to age one hundred taking into account sex, obesity, and presence of type-2 diabetes," *Clin. Anat.* **20**(8), 933–942 (2007).
23. M. Dharmalingam and P. G. Yamasandhi, "Nonalcoholic fatty liver disease and type 2 diabetes mellitus," *Indian J. Endocrinol. Metab.* **22**(3), 421 (2018).
24. L. Valenti et al., "Nonalcoholic fatty liver disease: cause or consequence of type 2 diabetes?," *Liver Int.* **36**(11), 1563–1579 (2016).
25. P. Nasr et al., "The amount of liver fat predicts mortality and development of type 2 diabetes in non-alcoholic fatty liver disease," *Liver Int.* **40**(5), 1069–1078 (2020).
26. C. Nadarajah et al., "Association of pancreatic fat content with type II diabetes mellitus," *Clin. Radiol.* **75**(1), 51–56 (2020).
27. A. Misra et al., "Effect of supervised progressive resistance-exercise training protocol on insulin sensitivity, glycemia, lipids, and body composition in Asian Indians with type 2 diabetes," *Diabetes Care* **31**(7), 1282–1287 (2008).
28. C. F. Baker, K. Overvad, and C. C. Dahm, "Lean body mass and risk of type 2 diabetes—a Danish cohort study," *J. Diabetes Metab. Disord.* **18**(2), 445–451 (2019).
29. S. K. J. Rehunen et al., "A high lean body mass is not protecting from type 2 diabetes in the presence of a high body fat mass," *Diabetes Metab.* **47**(6), 101219 (2021).
30. K. Xu et al., "AI body composition in lung cancer screening: added value beyond lung cancer detection," *Radiology* **308**(1), e222937 (2023).
31. P. Borrelli et al., "Artificial intelligence-aided CT segmentation for body composition analysis: a validation study," *Eur. Radiol. Exp.* **5**(1), 11 (2021).
32. M. H. Lee et al., "Abdominal CT body composition thresholds using automated AI tools for predicting 10-year adverse outcomes," *Radiology* **306**(2), e220574 (2023).
33. B. Wang and M. Torriani, "Artificial intelligence in the evaluation of body composition," *Semin. Musculoskelet. Radiol.* **24**(1), 30–37 (2020).
34. B. D. Pooler et al., "Technical adequacy of fully automated artificial intelligence body composition tools: assessment in a heterogeneous sample of external CT examinations," *Am. J. Roentgenol.* **221**(1), 124–134 (2023).
35. K. Magudia et al., "Utility of normalized body composition areas, derived from outpatient abdominal CT using a fully automated deep learning method, for predicting subsequent cardiovascular events," *Am. J. Roentgenol.* **220**(2), 236–244 (2023).
36. R. Strand et al., "A concept for holistic whole body MRI data analysis, Imiomics," *PLoS One* **12**(2), e0169966 (2017).
37. T. Kongara et al., "Determinants of pancreatic size and fat content in the UK Biobank: influence of race, genetic variants, and risk factors," *J. Clin. Endocrinol. Metab.* **110**(12), e3945–e3951 (2025).
38. J. Linge et al., "Body composition profiling in the UK Biobank imaging study," *Obesity* **26**(11), 1785–1795 (2018).
39. M. Jung et al., "Deep learning-based body composition analysis from whole-body magnetic resonance imaging to predict all-cause mortality in a large western population," *EBioMedicine* **110**, 105467 (2024).
40. J. Wasserthal et al., "TotalSegmentator: robust segmentation of 104 anatomic structures in CT images," *Radiol. Artif. Intell.* **5**(5), e230024 (2023).

41. T. Akinci D'Antonoli et al., "TotalSegmentator MRI: robust sequence-independent segmentation of multiple anatomic structures in MRI," *Radiology* **314**(2), e241613 (2025).
42. S. Lundberg and S.-I. Lee, "A unified approach to interpreting model predictions," arXiv:1705.07874 (2017).
43. I. Danciu et al., "Secondary use of clinical data: the Vanderbilt approach," *J. Biomed. Inform.* **52**, 28–35 (2014).
44. W. D. Bidgood et al., "Understanding and using DICOM, the data interchange standard for biomedical imaging," *J. Am. Med. Inform. Assoc.* **4**(3), 199–212 (1997).
45. J. Ashburner et al., "A (sort of) new image data format standard: NiFTI-1," https://nifti.nimh.nih.gov/nifti-1/documentation/hbm_nifti_2004.pdf (2004).
46. X. Li et al., "The first step for neuroimaging data analysis: DICOM to NIfTI conversion," *J. Neurosci. Methods* **264**, 47–56 (2016).
47. M. E. Kim et al., "Scalable quality control on processing of large diffusion-weighted and structural magnetic resonance imaging datasets," *PLoS One* **20**(8), e0327388 (2024).
48. J. J. M. van Griethuysen et al., "Computational radiomics system to decode the radiographic phenotype," *Cancer Res.* **77**(21), e104–e107 (2017).
49. J. Starekova et al., "Quantification of liver fat content with CT and MRI: state of the art," *Radiology* **301**(2), 250–262 (2021).
50. M. M. Shuey et al., "Next-generation phenotyping: introducing phecodeX for enhanced discovery research in medical phenomics," *Bioinformatics* **39**(11), btad655 (2023).
51. L. W. Remedios et al., "Lifespan pancreas morphology for control vs type 2 diabetes using AI on largescale clinical imaging," arXiv:2508.14878 (2025).
52. S. M. Lundberg, G. G. Erion, and S.-I. Lee, "Consistent individualized feature attribution for tree ensembles," arXiv:1802.03888 (2019).
53. F. Pedregosa et al., "Scikit-learn: machine learning in Python," https://www.jmlr.org/papers/volume12/pedregosa11a/pedregosa11a.pdf (2018).
54. L. McInnes, J. Healy, and J. Melville, "UMAP: uniform manifold approximation and projection for dimension reduction," arXiv:1802.03426 (2020).
55. X. Jin and J. Han, "K-means clustering," in *Encyclopedia of Machine Learning*, Springer, Boston, MA, pp. 563–564 (2011).
56. P. J. Rousseeuw, "Silhouettes: a graphical aid to the interpretation and validation of cluster analysis," *J. Comput. Appl. Math.* **20**, 53–65 (1987).
57. S. Harada et al., "Associations of gestational diabetes and proton density fat fraction of vertebral bone marrow and paraspinal musculature in premenopausal women," *Front. Endocrinol.* **14**, 1303126 (2024).

Lucas W. Remedios is a PhD student in computer science at Vanderbilt University. His research focuses on artificial intelligence in medical imaging domains. He is advised by Dr Bennett Landman.

Biographies of the other authors are not available.